Mechanical Properties and Morphologies of Polypropylene Composites Synergistically Filled by Styrene-Butadiene Rubber and Silica Nanoparticles

Wei-Zhi Wang, Tianxi Liu

Key Laboratory of Molecular Engineering of Polymers of Ministry of Education, Department of Macromolecular Science, Fudan University, 220 Handan Road, Shanghai 200433, People's Republic of China

Received 14 April 2007; accepted 24 December 2007
DOI 10.1002/app.28021
Published online 23 April 2008 in Wiley InterScience (www.interscience.wiley.com).

ABSTRACT: The mechanical properties and morphologies of PP/SBR/SiO_2 nanocomposites have been studied using mechanical testing, wide-angle X-ray diffraction (WAXD), polarizing optical microscopy (POM), scanning electron microscopy (SEM), differential scanning calorimetry (DSC), and thermogravimetric analysis (TGA). The mechanical properties of neat polypropylene can be considerably improved by synergistically filling with SiO_2 and SBR nanoparticles, especially for the notched Izod impact strength. The results from the WAXD, POM, SEM, DSC, and TGA measurements reveal that: (i) the β-phase crystal structure of PP is formed when SiO_2 and SBR nanoparticles are synergistically filled with polypropylene and its formation plays a role for the enhancement of the impact strength for PP/SBR/SiO_2 nanocomposites; (ii) the dispersion of SiO_2 and SBR nanoparticles in PP/SBR/SiO_2 composites is homogeneous, indicating that synergistic incorporating method decreases the aggregation of nanoparticles and thus increases the sites for dissipation of shock for impact energy in PP/SBR/SiO_2 nanocomposites; (iii) the thermal analysis shows high thermal stability for the PP/SBR/SiO_2 nanocomposites. © 2008 Wiley Periodicals, Inc. J Appl Polym Sci 109: 1654–1660, 2008

Key words: polypropylene; rubber; nanocomposites; mechanical properties; morphology

INTRODUCTION

Polypropylene (PP) as a kind of thermoplastics is widely used in many fields, such as building materials, furniture, automobiles, and toy industry. However, the main disadvantage of PP is its poor impact resistance, especially at low temperature. Therefore, PP is usually modified with elastomers to improve its impact strength,[1–6] which enhances the toughness of PP/rubber blends, however, at the same time always accompanies the sacrifice of the stiffness. In recent years, the inorganic nanoparticle-filled composites have been widely studied and developed rapidly, which could provide an alternative to increase both the stiffness and the toughness at the same time.[7–12] However, there exist several important issues when fabricating these polymer nanocomposites, such as the difficulty of achieving homogeneous dispersion of nanoparticles in a polymeric matrix due to the strong tendency of nanoparticles to agglomerate, and thus low loading level of the reinforcing fillers.[13] To solve these problems, many researchers focused on the studies of *in situ* polymerization of monomers in the presence of nanoparticles,[14–16] such as the sol–gel process and the intercalation polymerization technique.[17,18] Although nanoscale dispersion of the particles can be obtained using these methods, they are not suitable to produce nanocomposites in mass with low cost and applicability. Recently, Zhang reported that styrene-butadiene rubber (SBR) nanoparticles could be used to toughen PP.[19] However, the inhomogeneous dispersion and incorporation of low loading level of nanoparticles in PP only increase the toughness and stiffness of composites moderately.

In the present article, we combine the stiffness of inorganic (silica) nanoparticles and the toughness of (styrene-butadiene) rubber nanoparticles in PP matrix to overcome the disadvantages existing in the abovementioned methods. Furthermore, certain interparticle distance or space could be formed between the two different nanoparticles when they are mixed together and incorporated into PP matrix.[20] Owing to the increased distance between the same nanoparticles, PP can penetrate the agglomerated nanoparticles easily and thus greatly enhance the dispersion state of the nanoparticles. In this

Correspondence to: W. Z. Wang (weizhiwang@fudan.edu.cn); T. X. Liu (txliu@fudan.edu.cn).

Contract grant sponsor: Shanghai Leading Academic Discipline Project; contract grant number: B113.

Contract grant sponsor: The Program for Changjiang Scholars and Innovative Research Team in University (PCSIRT).

Journal of Applied Polymer Science, Vol. 109, 1654–1660 (2008)

TABLE I
Optimizing the Formulation Using Orthogonal Experiments for Three Series Of Nanocomposites

Sample code	Component weight (g)[a]			Tensile strength (MPa)	Elongation at break (%)	Modulus (MPa)	Impact strength (kJ/m^2)
	PP	SiO_2	SBR				
1	80 (1)	3 (1)	4 (1)	40.9	153	927	6.7
2	90 (2)	3 (1)	7 (2)	39.2	150	874	7.4
3	100 (3)	3 (1)	10 (3)	38.1	124	777	5.6
4	80 (1)	5 (2)	7 (2)	38.8	84	841	10.3
5	90 (2)	5 (2)	10 (3)	37.7	73	971	5.9
6	100 (3)	5 (2)	4 (1)	41.0	174	909	6.6
7	80 (1)	8 (3)	10 (3)	38.3	35	972	5.2
8	90 (2)	8 (3)	4 (1)	41.3	72	964	5.3
9	100 (3)	8 (3)	7 (2)	39.9	43	1010	6.2

[a] The component weights are listed outside the parentheses. The test level numbers of orthogonal experiments are listed inside the parentheses.

work, the preparation, the mechanical properties and the morphologies of PP/SBR/SiO_2 nanocomposites are investigated to clarify the relationship between the structure and the mechanical properties.

EXPERIMENTAL

Materials and sample preparation

PP resin (commercial name F401, melt flow rate 2.7, M_n = 55,000) was supplied by Yangzi Petrochemical Co., China. Ultrafine and fully vulcanized SBR nanoparticles (with 50 wt % butadiene and average size of 100 nm) were supplied by SINOPEC Beijing Research Institute of Chemical Industry, China. Silica nanoparticles (with size of 20 nm) were obtained from the Zhoushan Corp., China. All chemicals were used as received without any purification.

PP was mixed with SiO_2 and SBR nanoparticles in an SJSH-30 twin-screw extruder (Nanjing Plastic and Rubber Factory, China) with a barrel temperature of 190°C and screw speed of 200 rpm, according to the formulation listed in Table I. The samples used for the subsequent measurements were obtained by injection molding.

Characterization

The tensile properties were measured with a Universal Testing Machine (DCS5000, Shimadzu, Japan) at 25 ± 2°C. The crosshead speed was set to be 50 mm/min. The dumb-bell shaped specimens were prepared according to ASTM D412-87. The notched Izod impact strength (NIIS) was measured using an Izod impact tester (made in Chengde, China). The sample size of the rectangular specimens was 80 × 10 × 4 mm^3 with a 45° V-shaped notch (with tip radius of 0.25 mm and depth of 2 mm). The data reported here were averaged using the values from five specimens tested.

Wide-angle X-ray diffraction (WAXD) measurements were recorded at room temperature with a D/Max-rA rotating anode X-ray diffractometer (Rigaku Electrical Machine Company, Japan) equipped with a Cu Kα tube and Ni filter. The diffraction patterns were obtained over a range of diffraction angle of 2θ = 10–40° under a voltage of 40 kV and a current of 50 mA. Polarizing optical micrographs (POM) were obtained using a Nikon-YS2 optical microscope (Nikon, Japan) with sample thickness of about 50 μm. Scanning electron microscopy (SEM) observations were performed using a Hitachi X650 scanning electron microscope. Prior to SEM observations, the samples were etched by xylene and then coated with a conductive gold layer. Differential scanning calorimetry (DSC) data were obtained in nitrogen atmosphere at a heating rate of 10°C/min using a Perkin–Elmer differential scanning calorimeter (model DSC-2). The degree of crystallinity of PP in the nanocomposites was evaluated from the ratio of the fusion heat values of the composites to the fusion heat of neat PP (ΔH_{PP} = 209 J/g).[21] Thermal stability was estimated with a thermogravimetric analyzer (TGA) (Perkin–Elmer TGA7) over a temperature range between ambient temperature and 800°C at a heating rate of 10°C/min. All the samples for POM and WAXD experiments were prepared by hot-pressing at 190°C into films with thickness of about 100 μm, followed by slowly cooling to room temperature.

Orthogonal experiments

An orthogonal array was employed in this study as a tool for systematic experimental design. Experiments using an orthogonal array allow several effects of factors to be simultaneously determined efficiently. A matrix experiment consists of a set of experiments in which the settings of various process factors change from row to row according to the or-

TABLE II
Orthogonal Experiments Data Analysis for Table I

Sample code	Component weight (g)			Tensile strength (MPa)	Elongation at break (%)	Modulus (MPa)	Impact strength (kJ/m^2)
	PP	SiO_2	SBR				
PP/SiO_2/SBR	80	5	7	38.8	84	841	10.3
PP/SiO_2	80	5	0	44.0	40	1005	7.8
PP/SBR	80	0	7	34.1	324	820	6.0
PP	100	0	0	34.0	28	812	3.0

thogonal array, similar to the test level numbers of orthogonal experiments listed inside the parentheses in Table I and the three rows in Table II. One of the advantages of utilizing orthogonal array is the simplicity of data analysis. The effects of the various factors can be determined by computing simple averages. Another advantage is that it produces more reliable estimates on the effects of the factors with fewer experiments than those of the traditional methods, e.g., the experiments with one factor each time. Consequently, much fewer numbers of experiments are required.

RESULTS AND DISCUSSION

Optimizing formulation of PP nanocomposites

Table I listed a series of PP/SBR/SiO_2 nanocomposites that were designed and formulated according to an orthogonal table. The analysis data of Table I were listed in Table II. From Tables I and II it can be seen that: (i) increasing the content of PP increases the elongation at break and the tensile strength (TS), but decreases the notched Izod impact strength (NIIS) and the modulus of nanocomposites; (ii) increasing the content of SiO_2 nanoparticles increases the TS and the modulus, but decreases the elongation at break and the NIIS of the nanocomposites; (iii) SBR nanoparticles can decrease the TS, the elongation at break, the modulus, and the NIIS. However, it should be noted that for the test level of 2 in the cases of both SiO_2 and SBR, the value of the NIIS shows the maximum, as shown in Table II. The results show that the formulation of sample 4 significantly improves the NIIS of PP matrix. Therefore, the test level of 2 was the optimization condition for both SiO_2 and SBR. Consequently, PP/SBR/SiO_2 nanocomposite of sample 4 was selected and studied in the following section. For sample 4, the NIIS of the nanocomposite was significantly improved upon incorporation of SiO_2 and SBR into PP matrix.

Mechanical properties of PP nanocomposites

Table III lists the weight of each component, the TS, the elongation at break, the modulus, and the NIIS data of neat PP and its SBR/SiO_2, SiO_2, and SBR nanocomposites. It shows that the TS, the elongation at break, the modulus, and the NIIS of PP/SiO_2 nanocomposite are 44.0 MPa, 40%, 1005 MPa, and 7.8 kJ/m^2, respectively. The corresponding values of PP/SBR nanocomposites are 34.1 MPa, 324%, 820 MPa, and 6.0 kJ/m^2, respectively. These results reflect the nature of the stiff SiO_2 and the tough SBR nanoparticles. Compared with neat PP, the SiO_2 or SBR nanoparticles can improve the toughness and stiffness of matrix simultaneously. The values of the TS, the elongation at break, and the modulus of PP/SiO_2/SBR nanocomposites are between those of the PP/SBR and PP/SiO_2 composites, which is different from the case of the NIIS. The NIIS of PP/SBR/SiO_2 nanocomposite is 10.3 kJ/m^2, which is higher than that of PP/SBR or PP/SiO_2 systems, as shown in Table III. It is attributed to the synergistic effect upon incorporating both rigid SiO_2 nanoparticles and flexible SBR nanoparticles.

The toughening mechanisms using nanoparticles can be mainly attributed to two reasons. Firstly, the SBR nanoparticles act as stress concentration sites for dissipation of shock or impact energy by controlling and promoting matrix deformation. The addition of rubber particles into PP leads to relaxation of the

TABLE III
The Mechanical Properties of the Samples

Sample code	Component weight (g)			Tensile strength (MPa)	Elongation at break (%)	Modulus (MPa)	Impact strength (kJ/m^2)
	PP	SiO_2	SBR				
PP/SiO_2/SBR	80	5	7	38.8	84	841	10.3
PP/SiO_2	80	5	0	44.0	40	1005	7.8
PP/SBR	80	0	7	34.1	324	820	6.0
PP	100	0	0	34.0	28	812	3.0

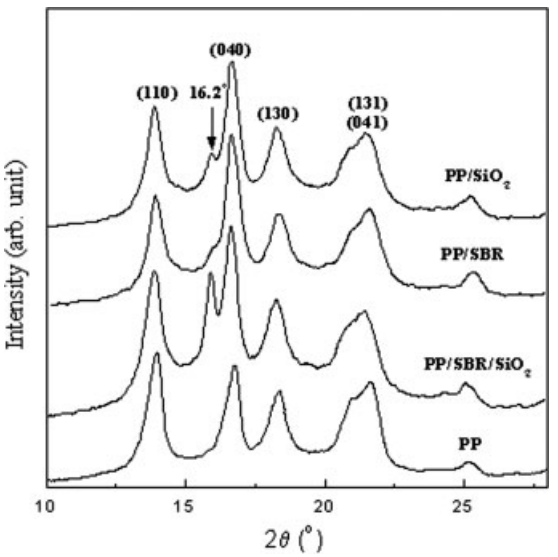

Figure 1 WAXD patterns of neat PP, and PP/SBR/SiO_2, PP/SiO_2, PP/SBR nanocomposites.

stress concentration and suppresses the formation of the matrix crazes or deformation. Secondly, the addition of SiO_2 nanoparticles further improves the fine dispersion of SBR nanoparticles and thus decreases the possibility of rubber cohesion into bulky particles during the mechanical mixing process. As a result, the sites for dissipation of shock or impact energy (i.e., the impact strength) are greatly increased in the PP/SBR/SiO_2 nanocomposites.

Crystal structures of PP in the nanocomposites

The WAXD spectra of neat PP, PP/SBR/SiO_2, PP/SiO_2, and PP/SBR nanocomposites are shown in Figure 1. The reflection peaks at $2\theta = 14.1^\circ$, 16.8°, 18.5°, and 21.2° correspond to, (110), (040), (130), and the overlapped (131,041) planes, respectively, which are characteristics of α-type monoclinic crystal structures of PP.[22] It indicates that all the samples contain α-type crystals. However, in comparison to neat PP, it can be seen clearly that a new reflection at $2\theta = 16.2^\circ$ appears in all the three nanocomposites, especially for the PP/SBR/SiO_2 system. This new peak is assigned to (300) reflection of the β-type hexagonal crystal structure of PP. Moreover, the fraction of β-phase in the crystalline samples can be roughly estimated from the ratio of the height of (300) reflection of β-phase to the sum of the heights of the four reflections, i.e., (110), (040), and (130) of the α-phase and (300) of the β-phase, as proposed by Turner-Jones.[23] The calculated results of β-phase fraction for PP/SBR/SiO_2, PP/SBR, and PP/SiO_2 nanocomposites are 24.0%, 13.7%, and 15.8%, respectively. It shows that the fractions of β-phase in PP/SiO_2 and PP/SBR samples are less than that in PP/SBR/SiO_2 sample, probably due to the synergistic nucleating effect of SBR and SiO_2 nanoparticles in PP matrix. The appearance of β-type hexagonal crystals obviously improves the impact strength of PP because the β-type hexagonal crystals have higher ductility and strength than the α-type monoclinic crystals.[24] These results are also confirmed by the mechanical measurements mentioned above.

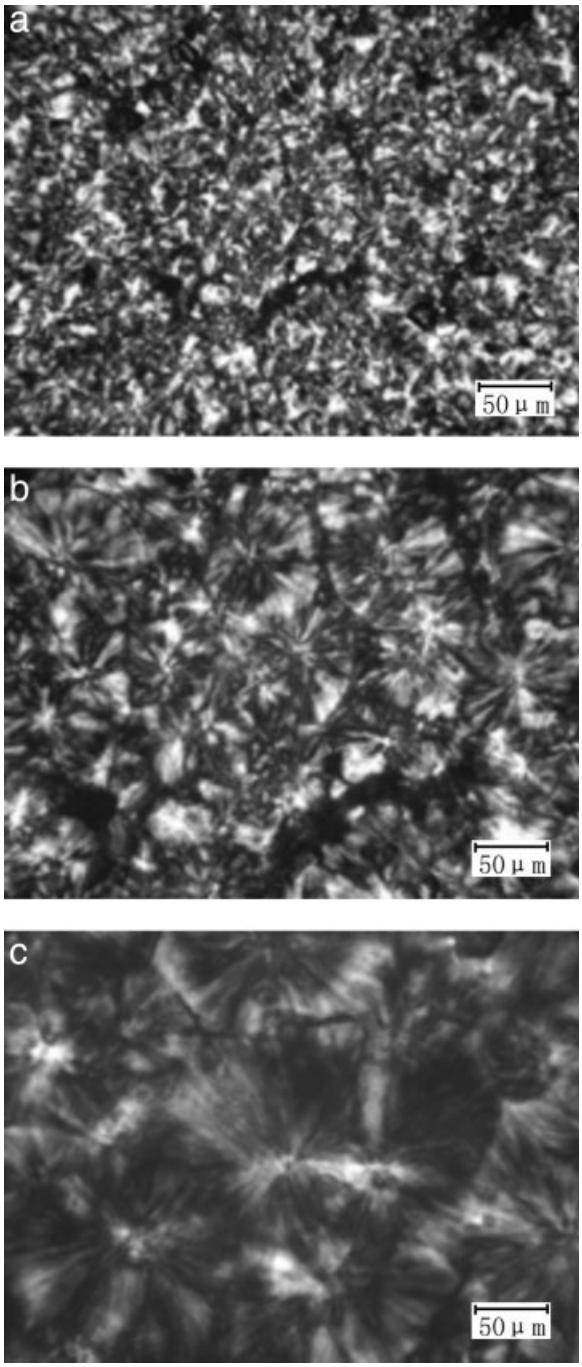

Figure 2 POM images of different nanocomposites: (a) PP/SBR/SiO_2, (b) PP/SiO_2, (c) PP/SBR.

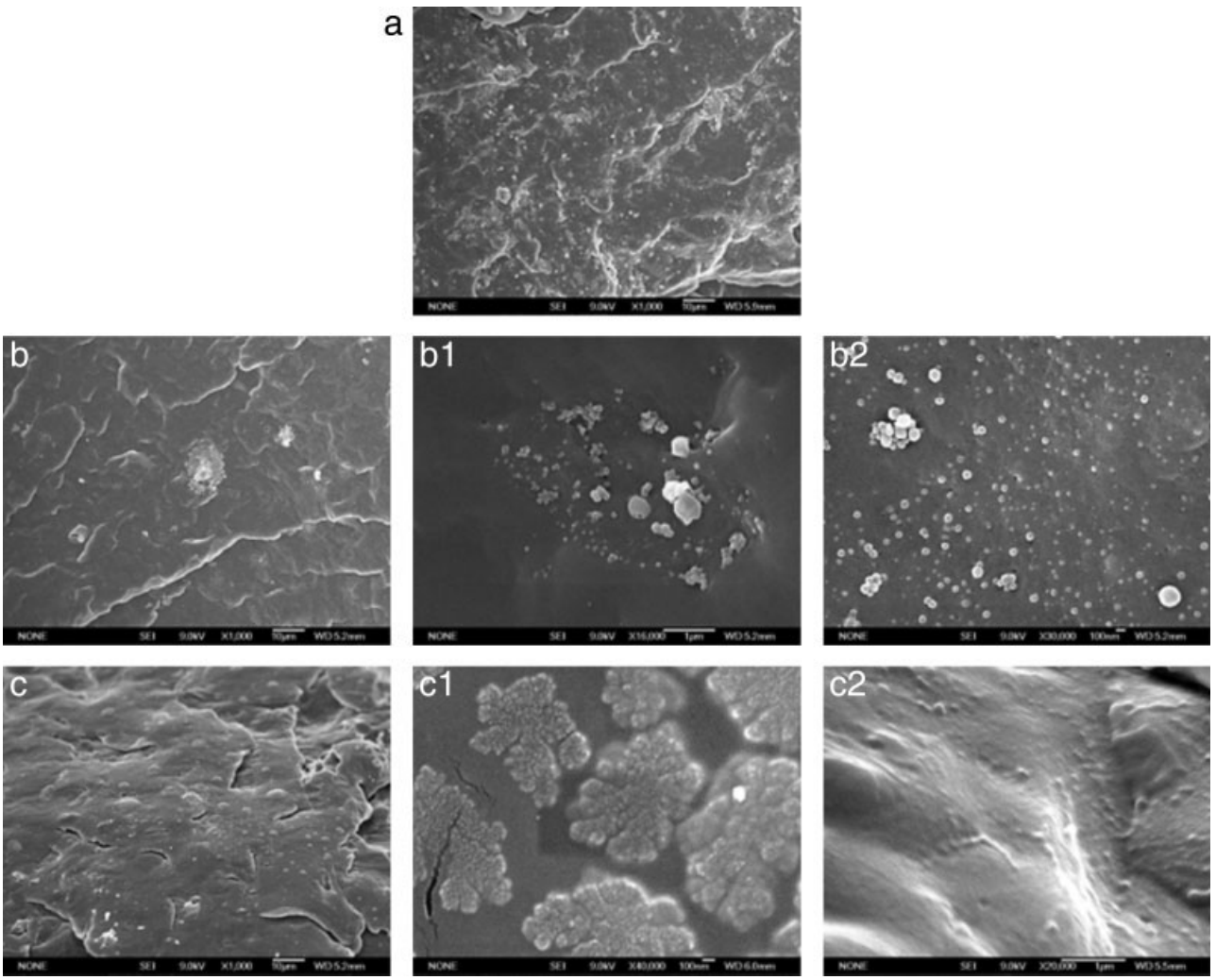

Figure 3 SEM micrographs of the nanocomposites: (a) and (a_1) for PP/SBR/SiO_2; (b), (b1), and (b2) for PP/SiO_2; (c), (c1), and (c2) for PP/SBR.

Figure 2 shows the POM images of the nanocomposites. Figure 2(a,b,c) are for PP/SBR/SiO_2, PP/SiO_2, and PP/SBR samples, respectively. Figure 2(a) clearly shows that the spherulites of PP in PP/SBR/SiO_2 composites are imperfect or much less developed and the spherulite size significantly decreases when compared with those of PP/SiO_2 [Fig. 2(b)] and PP/SBR [Fig. 2(c)] composites. It thus indicates that incorporating SiO_2 and SBR nanoparticles into the matrix makes the spherulites imperfect and also induces the formation of the β-type hexagonal crystals of PP. And the increase of the β-type crystal fraction is favorable to the improvement of the toughness of PP matrix.

Morphologies of PP nanocomposites

Figure 3 shows the fractured surfaces of the nanocomposites by SEM at different magnifications. For PP/SBR/SiO_2 sample, Figure 3(a) shows a continuous PP matrix in which SiO_2 and SBR nanoparticles are dispersed homogeneously. Figure 3(a1) is the same sample as Figure 3(a) but at a higher magnification, which clearly shows the homogeneous dispersion of nanoparticles. The large and irregular particles visible in Figure 3(a1) are the crosslinked SBR particles which can not be etched by xylene due to the gelled nature of the network. The small round particles between SBR particles are SiO_2 particles which are finely dispersed without noticeable agglomeration. The SBR particles are also homogeneously dispersed in PP matrix. The synergistically filled SiO_2 and SBR particles into PP can improve their dispersions due to the interval effects. Figures 3(b,b1,b2) show the fractured surface of PP/SiO_2 sample at different magnifications. Figures 3(b1,b2) show two typical (enlarged) clusters. The aggregation or cluster of SiO_2 particles is clearly observed and the dispersion of SiO_2 nanoparticles in Figure 3(b2) is more homogeneous than that in Figure 3(b1). However, poor dispersion of SiO_2 particles in some regions of the fractured surface can also be

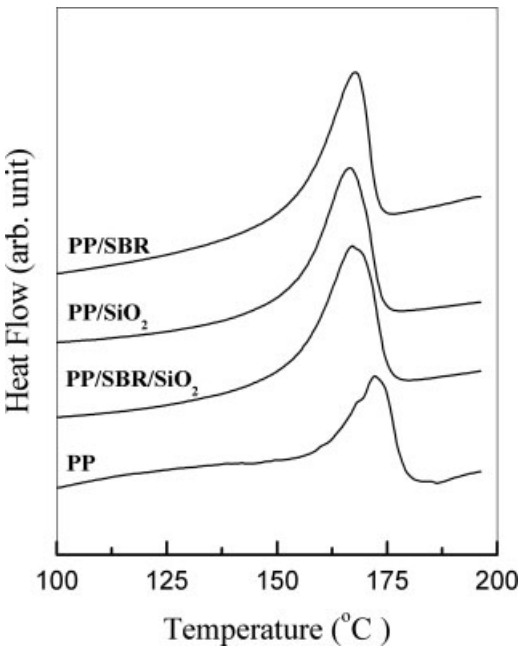

Figure 4 DSC curves of PP, PP/SBR/SiO_2, PP/SiO_2, and PP/SBR nanocomposites.

observed in PP matrix, and the existence of SiO_2 cluster results in the destruction of matrix when PP/SiO_2 nanocomposite is deformed by impact strength. Figure 3(c) shows the fractured sample of PP/SBR sample. The morphology of SBR particles can be divided into two situations. Some particles are well dispersed in PP matrix with small size as shown in Figure 3(c2). This is because the particles are easily broken into smaller ones and are dispersed homogeneously into PP under the condition of high mixing torque. And some other particles aggregate to form clusters due to poor compatibility with PP, as shown in Figure 3(c1). The existence of SBR clusters cannot improve the toughness of PP/SBR effectively. The above results provide distinct evidence that SiO_2 and SBR nanoparticles can synergistically improve their dispersion state within PP matrix.

Thermal analysis of PP nanocomposites

Figure 4 shows the DSC melting curves for PP/SBR, PP/SiO_2, and PP/SBR/SiO_2 nanocomposites over the temperature range of 100–200°C. It can be seen that the melting peaks shift toward lower temperatures for PP/SBR/SiO_2, PP/SiO_2, PP/SBR samples in contrast to that of neat PP. This is probably because the addition of nanoparticles plays a role of nucleating agent and thus leads to the formation of small and imperfect PP crystals. This effect is more obvious in PP/SBR/SiO_2 nanocomposites than that in PP/SiO_2 or PP/SBR systems. The synergistic incorporation of SiO_2 and SBR nanoparticles into polypropylene improves their respective dispersion among the matrix, thus further inhibits the formation of perfect PP crystals. It can also be seen that the melting endotherm has a slight broadening in the DSC curves of the nanocomposites. This indicates that the presence of nanoparticles acting as nucleation agent induces the formation of β-type crystals of PP, and therefore the coexistence of the α-type and β-type crystals in the nanocomposites results in the broadening of melting endotherm. The DSC results of melting behavior and crystallinity of the samples are listed in Table IV. It shows that the crystallinity of PP/SBR/SiO_2 sample is higher than those of PP/SBR and PP/SiO_2 samples, probably due to the formation of more β-type crystals in PP/SBR/SiO_2 sample. The above results from thermal analysis are consistent with those obtained from WAXD.

The thermal stability of neat PP and PP/SBR, PP/SiO_2, and PP/SBR/SiO_2 nanocomposites is estimated using thermogravimetric analysis (TGA) over the temperature range of 20–800°C. And the data of initial degradation temperature (T_{id}), the 5% weight loss degradation temperature (T_d), and the total weight loss of all the samples by TGA are summarized in Table V. It can be clearly seen that the thermal stability of PP/SBR system is only slightly improved in comparison to that of neat PP. However, the thermal degradation temperatures of PP/SiO_2 system are significantly increased, probably due to the inorganic nature of SiO_2 nanoparticles. The presence of inorganic silica particles hinders the outdiffusion of the volatile degraded products. And the most significant increase of the T_{id} and T_d (by about 70°C) is observed for PP/SBR/SiO_2 system, due to the synergistic incorporation of both SiO_2 and SBR nanoparticles into PP matrix.

TABLE IV
Melting Behavior and Crystallinity of Neat PP, PP/SBR, PP/SiO_2 and PP/SBR/SiO_2 Composites

Sample code	Component weight (g)			Tensile strength (MPa)	Elongation at break (%)	Modulus (MPa)	Impact strength (kJ/m^2)
	PP	SiO_2	SBR				
PP/SiO_2/SBR	80	5	7	38.8	84	841	10.3
PP/SiO_2	80	5	0	44.0	40	1005	7.8
PP/SBR	80	0	7	34.1	324	820	6.0
PP	100	0	0	34.0	28	812	3.0

TABLE V
TGA Data of Neat PP, PP/SBR, PP/SiO_2 and PP/SBR/SiO_2 Composites

Sample code	Component weight (g)			Tensile strength (MPa)	Elongation at break (%)	Modulus (MPa)	Impact strength (kJ/m^2)
	PP	SiO_2	SBR				
PP/SiO_2/SBR	80	5	7	38.8	84	841	10.3
PP/SiO_2	80	5	0	44.0	40	1005	7.8
PP/SBR	80	0	7	34.1	324	820	6.0
PP	100	0	0	34.0	28	812	3.0

CONCLUSIONS

The synergistic incorporation of SiO_2 and SBR nanoparticles into PP can significantly improve the mechanical properties of the matrix, especially for the notched Izod impact strength. The WAXD data show that the formation of β-type crystals of plays a role for the enhancement of the impact strength for PP/SBR/SiO_2 nanocomposites. SEM observations on the fractured surfaces of the composites demonstrate that the dispersion of SiO_2 and SBR nanoparticles in PP/SBR/SiO_2 composite is homogeneous. The synergistic filling approach greatly enhances the dispersion state of nanoparticles among the matrix thus increasing the sites for dissipation of shock for impact energy in PP/SBR/SiO_2 nanocomposites. The thermal analysis results show that PP/SBR/SiO_2 nanocomposite possesses higher thermal stability than that of PP/SiO_2 or PP/SBR systems.

References

1. George, S.; Varughese, K. T.; Thomas, S. Polymer 2000, 41, 5485.
2. Kim, J. Y.; Chun, B. C. J Mater Sci 2000, 35, 4833.
3. Tjong, S. C.; Li, W. D.; Li, R. K. Y. Eur Polym Mater 1998, 34, 755.
4. Wal, A. V. D.; Nijhof, R.; Gaymans, R. Polymer 1999, 40, 6031.
5. Tjong, S. C.; Xu, S. A.; Li, R. K. Y.; Mai, Y. W. Polym Int 2002, 51, 1248.
6. Tjong, S. C.; Xu, S. A.; Mai, Y. W. Polym Compos 2003, 24, 437.
7. Jain, A. K.; Nagpal, A. K.; Singhal, R. J Appl Polym Sci 2089 2000, 78.
8. Gupta, N. K.; Jain, A. K.; Singhal, R. J Appl Polym Sci 2000, 78, 2104.
9. Inoue, T.; Suzuki, T. J Appl Polym Sci 1995, 56, 1113.
10. Kim, B. K.; Choi, C. H. J Appl Polym Sci 1996, 60, 2199.
11. Ha, C. S.; Kim, S. C. J Appl Polym Sci 1998, 35, 2211.
12. Ruan, W. H.; Huang, X. B.; Wang, X. H.; Rong, M. Z.; Zhang, M. Q. Macromol Rapid Commun 2006, 27, 581.
13. Wu, C. L.; Zhang, M. Q.; Rong, M. Z.; Friedrich, K. Compos Sci Technol 2002, 62, 1327.
14. Cai, L. F.; Huang, X. B.; Rong, M. Z.; Ruan, W. H.; Zhang, M. Q. Polymer 2006, 47, 7043.
15. Friedrich, K.; Rong, M. Z.; Zhang, M. Q.; Ruan, W. H. Key Eng Mater 2006, 312, 229.
16. Zhou, H. J; Rong, M. Z.; Zhang, M. Q.; Lehmann, B.; Friedrich, K. Polym J 2006, 37, 677.
17. Novak, B. M. Adv Mater 1993, 5, 422.
18. Giannelis, E. P. Adv Mater 1996, 8, 29.
19. Zhang, M.; Liu, Y.; Zhang, X. Polymer 2002, 43, 5133.
20. Andrew, J R.; Mai, Y. W. Mater Sci Eng A 1999, 265, 202.
21. Chang, S. H.; Dong, J. I.; Sung, C. K. J. Appl Polym Sci 1986, 32, 6281.
22. Wang, W. Z.; Wu, Q. H.; Qu, B. J Polym Eng Sci 2003, 43, 1497.
23. Turner, A. J.; Aizlewood, J. M.; Beckett, D. R. Makromol Chem 1964, 75, 134.
24. Zhang, W. Acta Polym Sin 1992, 1, 61.